

## Article

# Power Phase Apodization Study on Compensation Defocusing and Chromatic Aberration in the Imaging System

Svetlana N. Khonina <sup>1,2,\*</sup> , Sergey G. Volotovskiy <sup>1</sup>, Alexey P. Dzyuba <sup>3</sup>, Pavel G. Serafimovich <sup>1</sup>,  
Sergey B. Popov <sup>1,2</sup> and Muhammad A. Butt <sup>2,4</sup> 

<sup>1</sup> Image Processing Systems Institute of RAS-Branch of the FSRC “Crystallography and Photonics” RAS, 151 Molodogvardeyskaya Str., 443001 Samara, Russia; sv@ipsiras.ru (S.G.V.); paulserch05@gmail.com (P.G.S.); sepo@ipsiras.ru (S.B.P.)

<sup>2</sup> Faculty of Information Technology, Samara National Research University, 34 Moskovskoye Shosse, 443086 Samara, Russia; butt.m@ssau.ru

<sup>3</sup> ITMO University, 49 Kronverksky Av., 197101 St. Petersburg, Russia; poseydon.iq@gmail.com

<sup>4</sup> Institute of Microelectronics and Optoelectronics, Warsaw University of Technology, Koszykowa 75, 00-662 Warszawa, Poland

\* Correspondence: khonina@ipsiras.ru

**Abstract:** We performed a detailed comparative study of the parametric high degree (cubic, fourth, and fifth) power phase apodization on compensation defocusing and chromatic aberration in the imaging system. The research results showed that increasing the power degree of the apodization function provided better independence (invariance) of the point spread function (PSF) from defocusing while reducing the depth of field (DOF). This reduction could be compensated by increasing the parameter  $\alpha$ ; however, this led to an increase in the size of the light spot. A nonlinear relationship between the increase in the DOF and spot size was shown (due to a small increase in the size of the light spot, the DOF can be significantly increased). Thus, the search for the best solution was based on a compromise of restrictions on the circle of confusion (CoC) and DOF. The modeling of color image formation under defocusing conditions for the considered apodization functions was performed. The subsequent deconvolution of the resulting color image was demonstrated.

**Keywords:** imaging system; extended depth of field; power phase apodization; image deconvolution



check for updates

**Citation:** Khonina, S.N.; Volotovskiy, S.G.; Dzyuba, A.P.; Serafimovich, P.G.; Popov, S.B.; Butt, M.A. Power Phase Apodization Study on Compensation Defocusing and Chromatic Aberration in the Imaging System. *Electronics* **2021**, *10*, 1327. <https://doi.org/10.3390/electronics10111327>

Academic Editor: Gwanggil Jeon

Received: 30 April 2021

Accepted: 29 May 2021

Published: 1 June 2021

**Publisher's Note:** MDPI stays neutral with regard to jurisdictional claims in published maps and institutional affiliations.



**Copyright:** © 2021 by the authors. Licensee MDPI, Basel, Switzerland. This article is an open access article distributed under the terms and conditions of the Creative Commons Attribution (CC BY) license (<https://creativecommons.org/licenses/by/4.0/>).

## 1. Introduction

It is well known that conventional imaging systems are very sensitive to defocus and chromatic aberrations. An increase in the depth of field of the optical system makes it possible to weaken this sensitivity and its negative consequences of blurring defocused images. However, a simple increase in the depth of field (DOF) by reducing the pupil or numerical aperture of the system leads to a deterioration in resolution. One way to increase the DOF without degrading resolution is to “encode” the wavefront [1–6]. E.R. Dowski and W.T. Cathey proposed a wavefront coding technology based on the imaging lens complemented by a cubic-phase-modulation phase mask [1]. The additional phase mask changes the shape of the wavefront so that the modulus of the optical transfer function (MTF) of the system becomes independent of the defocusing [2,3]. In addition, the presence of the phase mask changes the point spread function (PSF) of the system, which now differs significantly from the Airy pattern. This distorts the image in focus, but now the PSF outside the focus is the same as the PSF in focus. Thus, the image is distorted in the same way at a very long interval [4]. It is possible to restore the image, which is now digitally independent of defocusing [5].

Such coding not only provides an increase in the depth of focus without the loss of resolution of the optical system but also allows the reduction of the influence of some types of aberrations, for example, chromatic [2,3] or off-axis aberrations [6,7]. The commonly

used cubic phase apodization of the exit pupil of the system was originally proposed in [1–3], but other types of phase functions have also been considered [8–15], including logarithmic functions [9], with varying degrees of dependence on the coordinate [11,13,15]. For example, in [15], a fractional degree was investigated. Optimization of multi-ring masks [11] and joint amplitude-phase apodization [12] were also considered.

Various methods of apodization have been known for a long time [16] and are widely used not only to increase the DOF but also to decrease the size of the focal spot [17–22]. Amplitude apodization is particularly well-known, in which the central part of the lens is screened, and radiation is only transmitted in the peripheral part of the lens [17,21,22]. A similar but more energetically effective result is achieved when a phase diffractive axicon is used as an apodizing element [23–25]. In both cases, a decrease in the focal spot size is accompanied by an increase in side lobes [26,27], which worsens the image properties. However, this drawback has little effect on the performance of scanning optical systems [28–31].

Interesting types of phase apodization include the use of a spiral phase plate to increase contrast in microscopes [32–34] as well as the application of asymmetric phase masks for resolving two nearby radiation sources [35–37].

In imaging systems, as a rule, the use of apodization requires an additional digital decoding operation [38–40]. Moreover, for color images, the task is somewhat more complicated [41,42]. Despite the development of various decoding methods, including neural networks [43–46], when optimizing the apodizing function, it is desirable to maintain a compromise between increasing the DOF and PSF distortion.

Among the various apodizing functions designed to increase the DOF, the cubic phase is used most often [1–3,47–50]. Other integer-power phase apodization functions are also convenient for decoding [11,13]. In addition to the degree of power, the properties of these functions can be significantly changed by one more parameter, namely, the scaling parameter. The combined effect of the degree of power and scale parameters on increasing the DOF and PSF distortion has not been previously studied.

In this paper, we considered high-order polynomial phase apodization (cubic, fourth, and fifth) and examined their properties, considering scale parameters in detail. This research aimed to optimize these parameters to increase the DOF with minimal PSF distortion and restriction on the circle of confusion (CoC). The research results showed that increasing the power degree of the apodization function provided better invariance of the PSF but a smaller increase of the DOF for the same interval of scaling parameters.

We also demonstrated the chromatic effect for polynomial phase apodization. The modeling of color image formation under defocusing conditions in presence of the apodization functions was performed. The subsequent deconvolution of the resulting color image demonstrated the possibility of obtaining very similar results for apodizing functions with different degrees of power due to variation of the scale parameter. However, a higher degree provided slightly better results with moderate defocus (20% of the focus value).

## 2. Theoretical Analysis of Polynomial Phase Apodization

Let us consider an imaging optical system consisting of one thin lens, the complex transmission function of which has the following form [51]:

$$l(x, y) = \text{circ}\left(\frac{r}{R}\right) \exp\left(-ik \frac{(x^2 + y^2)}{2f}\right), \quad (1)$$

where  $k = \frac{2\pi}{\lambda}$  is the wavenumber of the incident radiation with wavelength  $\lambda$ ,  $\text{circ}(\cdot)$  is the circular aperture of the  $R$  radius, and  $f$  is the focal length of the lens.

The focal length of a conventional refractive lens is dependent on the wavelength  $\lambda$  due to the chromatic dispersion of the refractive index of the lens material [52,53]. For a long-focus lens (with a focal length on the order of hundreds of millimeters), the focus

variations due to the chromatic dispersion are insignificant compared with the focus depth, which is estimated by the formula [52,53]

$$DOF \approx \frac{\lambda}{NA^2}, \quad (2)$$

where  $NA$  is the numerical aperture of the lens. In the paraxial case,  $NA = \frac{R}{f}$ , where  $R$  is the lens radius and  $f$  is the average focal length.

According to expression (2), the depth of field increases with decreasing numerical aperture, i.e., either with an increase in focal length or a decrease in the radius of the lens (or aperture). However, in this case, the resolution will deteriorate because the focal spot size, which can be estimated as the full width at half maximum (FWHM), is also inversely proportional to the numerical aperture of the system [52]:

$$FWHM \approx \frac{\lambda}{2NA}, \quad (3)$$

Phase apodization of the lens pupil (in contrast to reducing aperture) allows the depth of field to be increased without compromising resolution. However, in this case, the point spread function (PSF) is significantly different from the delta function and has significant side lobes. Visually, the image becomes very blurry, although it does not change when defocusing. To restore the image, an additional deconvolution operation is required.

The most famous is the cubic phase apodization [1–3,47–50]. In [10], asymmetric polynomial phase functions were considered, and [15] considered the general phase function:

$$\tau(x, y) = \exp\left\{i\alpha_0 \left[ \left(\frac{x}{R}\right)^q + \left(\frac{y}{R}\right)^q \right]\right\}, \quad (4)$$

where  $\alpha_0$  is the dimensionless variable parameter (which can be considered as a degree of freedom during optimization) and  $q$  is a positive real number.

In this paper, we conducted a comparative study of three asymmetric polynomial phase apodizations—cubic, fourth-, and fifth-degree:

$$p(x, y) = \exp\left\{ikR\alpha \cdot \text{Asym}\left[\left(\frac{x}{R}\right)^n + \left(\frac{y}{R}\right)^n\right]\right\}, \quad (5)$$

where  $\text{Asym}(\cdot)$  is the transforming function, which is introduced to form asymmetric distributions for even degrees  $n$ .

We recommend Equation (5) instead of (4) for the following reasons. Usually, when describing the complex transmission functions of elements such as an axicon  $\exp(ikar)$  and a lens  $\exp\left(-\frac{ikr^2}{2f}\right)$ , the wavenumber  $k$  is distinguished in the coefficients. For the axicon, the dimensionless parameter  $\alpha$  denotes the numerical aperture [54]. In Equation (5), the parameter  $\alpha$  also remains dimensionless, although it has a different meaning and is used to control field characteristics such as the DOF and FWHM.

To calculate the 3D PSF in the focal region and outside of it, we used the Fresnel transform [25]:

$$P(u, v, z) = -\frac{i}{\lambda z} \exp(ikz) \times \int_{-R}^R \int_{-R}^R l(x, y) p(x, y) \exp\left\{i\frac{k}{2z} [(u-x)^2 + (v-y)^2]\right\} dx dy. \quad (6)$$

Figure 1 (top row) shows the results of calculating the PSF for a lens with a focal length  $f = 100$  mm and a lens radius  $R = 3$  mm at the wavelength of the illuminating beam  $\lambda = 550$  nm. This figure shows that when defocusing, the PSF changes significantly, increasing in size.

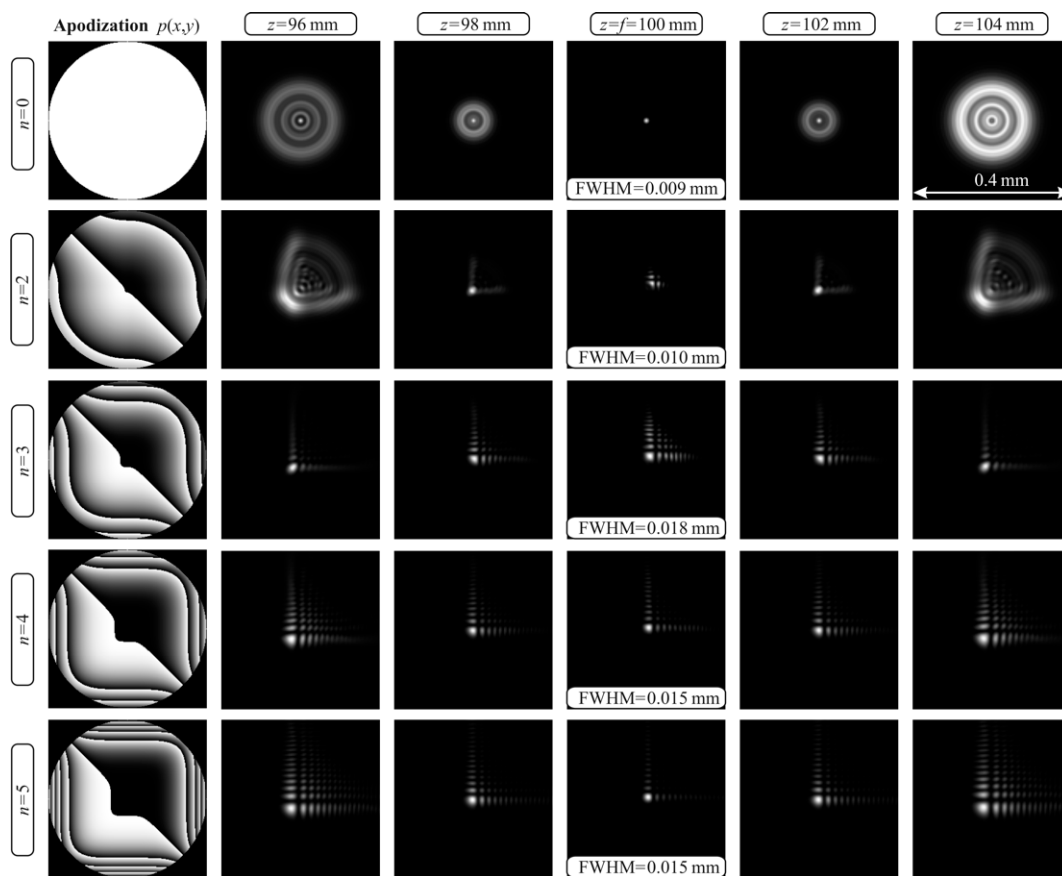


**Figure 1.** PSF with a CoC size limit of 0.02 mm at various distances (picture size  $0.4 \times 0.4 \text{ mm}^2$ ) for a lens without apodization (first row) and with asymmetric phase apodization of  $n = 2$ ,  $\alpha = 0.00025$  (second row);  $n = 3$ ,  $\alpha = 0.00045$  (third row);  $n = 4$ ,  $\alpha = 0.00054$  (fourth row); and  $n = 5$ ,  $\alpha = 0.00081$  (fifth row), with the wavelength of the illuminating beam  $\lambda = 550 \text{ nm}$ .

In the case of lens pupil apodization by a phase function using Equation (5) with  $n > 2$ , the PSF pattern changes much less, with a shift along the optical axis (the third, fourth, and fifth rows of Figure 1). However, at the same time, the PSF loses radial symmetry, and significant side lobes are formed.

The selection of the coefficient  $\alpha$  is carried out under the condition that the FWHM of the light spot (the main lobe of the PSF) is not more than 0.02 mm in the focal plane. This condition is associated with the limitation of the size of the central spot following the circle of confusion, which for serial cameras and photographic films varies from 0.02 mm to 0.08 mm [55]. Given this condition, the DOF can be estimated for each case.

For a more complete analysis of the influence of asymmetric apodization functions, we also considered the case  $n = 2$  (the second row of Figure 1). It should be noted that such an apodization was not successful. Even at small values of the parameter  $\alpha$ , the PSF structure changed noticeably, which was also clearly seen from the uneven longitudinal picture (Figure 2b); therefore, we did not consider this case further.

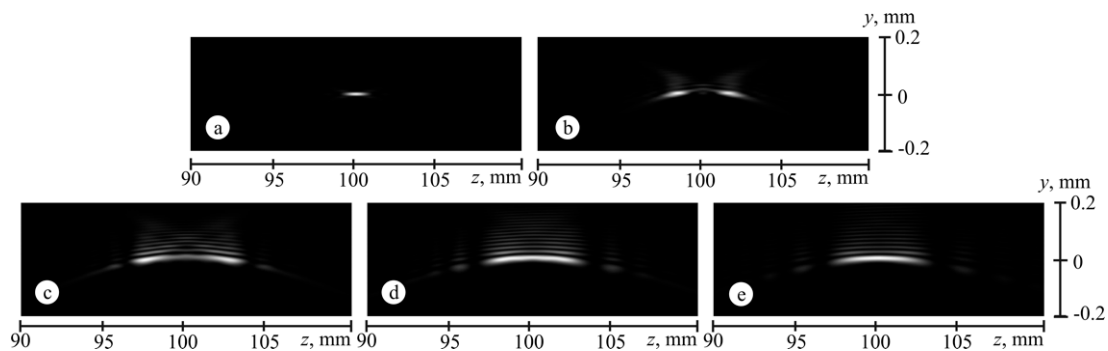


**Figure 2.** PSF longitudinal pattern with a CoC size limit of 0.02 mm ( $z \in [90 \text{ mm}; 110 \text{ mm}]$ ,  $y \in [-0.2 \text{ mm}; 0.2 \text{ mm}]$ ) for a lens without apodization (a) and with asymmetric phase apodization  $n = 2$ ,  $\alpha = 0.00025$  (b);  $n = 3$ ,  $\alpha = 0.00045$  (c);  $n = 4$ ,  $\alpha = 0.00054$  (d); and  $n = 5$ ,  $\alpha = 0.00081$  (e), with the wavelength of the illuminating beam  $\lambda = 550 \text{ nm}$ .

Figure 2 shows the longitudinal distribution of PSFs. For a lens without apodization,  $\text{DOF} = 1.1 \text{ mm}$  (Figure 2a); with asymmetric apodization  $n = 2$ ,  $\text{DOF} = 3.8 \text{ mm}$  (very uneven, Figure 2b); with  $n = 3$ ,  $\text{DOF} = 6.2 \text{ mm}$  (Figure 2c); with  $n = 4$ ,  $\text{DOF} = 5.3 \text{ mm}$  (Figure 2d); and with  $n = 5$ ,  $\text{DOF} = 4.6 \text{ mm}$  (Figure 2e). Thus, with increasing degrees  $n$ , the  $\text{DOF}$  decreases. However, apodizing functions of high degrees have advantages, particularly lower side lobes and smaller size of the central spot (Figure 1) as well as a more even distribution of longitudinal intensity (Figure 2).

For a more visual comparison, Figure 3 shows plots of horizontal sections of the corresponding PSF for apodizing functions of various degrees in the focal plane. For  $n = 4$  and  $n = 5$ , the level of the side lobes is significantly lower than for  $n = 3$ ; in addition, the size of the central spot is slightly smaller (Figure 3). This is important, as convolution with such a PSF will not distort the image visually.

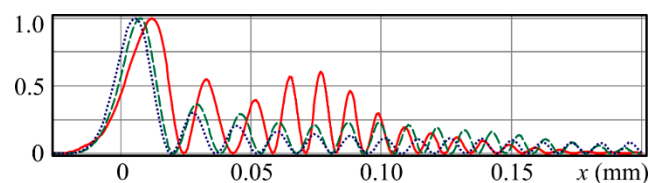


**Figure 3.** Normalized PSF cross-sections in the focal plane for a phase apodized lens  $n = 3$ ,  $\alpha = 0.00045$  (solid line,  $\text{FWHM} = 0.018 \text{ mm}$ );  $n = 4$ ,  $\alpha = 0.00054$  (dashed line,  $\text{FWHM} = 0.015 \text{ mm}$ );  $n = 5$ ,  $\alpha = 0.00081$  (dotted line,  $\text{FWHM} = 0.015 \text{ mm}$ ).

Note that apodizing function (5), in addition to degree  $n$ , has one more parameter, the coefficient  $\alpha$ , which can also be used to control the properties of PSF. Figure 4 shows the simulation results for phase apodized lenses with  $n = 5$  for different values of  $\alpha$ :  $\alpha = 0.002$  ( $\text{DOF} = 6.5 \text{ mm}$ ,  $\text{FWHM} = 0.018 \text{ mm}$ ),  $\alpha = 0.005$  ( $\text{DOF} = 9.4 \text{ mm}$ ,  $\text{FWHM} = 0.022 \text{ mm}$ ), and  $\alpha = 0.01$  ( $\text{DOF} = 12.3 \text{ mm}$ ,  $\text{FWHM} = 0.025 \text{ mm}$ ). This shows that with an increase in the coefficient  $\alpha$ , the length of the PSF invariance ( $\text{DOF}$ ) increases, although the size of the central spot also increases slightly.

Note that for  $n = 3$  and  $\alpha = 0.00045$ , we obtain  $\text{DOF} = 6.2 \text{ mm}$  and  $\text{FWHM} = 0.018 \text{ mm}$  (Figure 2c), and for  $n = 5$  and  $\alpha = 0.002$ , we obtain  $\text{DOF} = 6.5 \text{ mm}$  and  $\text{FWHM} = 0.018 \text{ mm}$  (Figure 4a). Thus, practically the same characteristics were obtained with different apodizations. In addition, the PSF pattern for  $n = 5$  appears smoother than that for  $n = 3$ . Thus, when choosing the apodizing function, it is possible to focus on a compromise between increasing the  $\text{DOF}$  and distorting PSF.

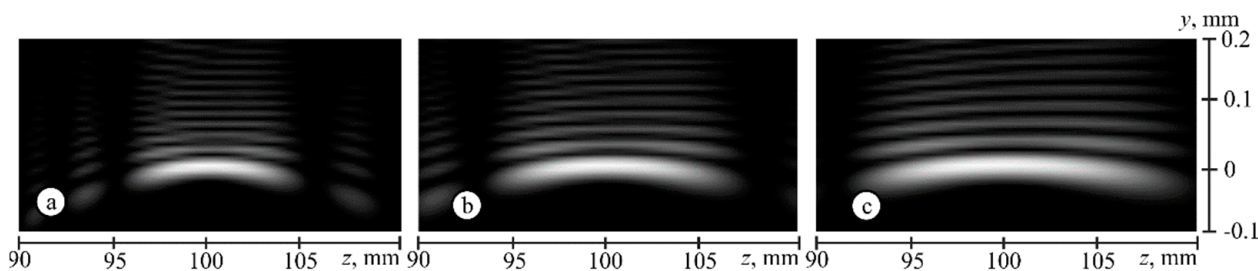


**Figure 4.** PSF longitudinal pattern for phase apodized lenses  $n = 5$  ( $z \in [90 \text{ mm}; 110 \text{ mm}]$ ,  $y \in [-0.1 \text{ mm}; 0.2 \text{ mm}]$ ):  $\alpha = 0.002$  (a),  $\alpha = 0.005$  (b) and  $\alpha = 0.01$  (c) at the wavelength of the illuminating beam  $\lambda = 550 \text{ nm}$ .

To determine the possible set of parameters of the apodization function (5) for the given characteristics, we examined the dependence of the central light spot size in the focal plane and the DOF on the coefficient  $\alpha$  (Figure 5). This demonstrates that the dependencies for different degrees  $n$  are similar, but they differ in quantitative characteristics.

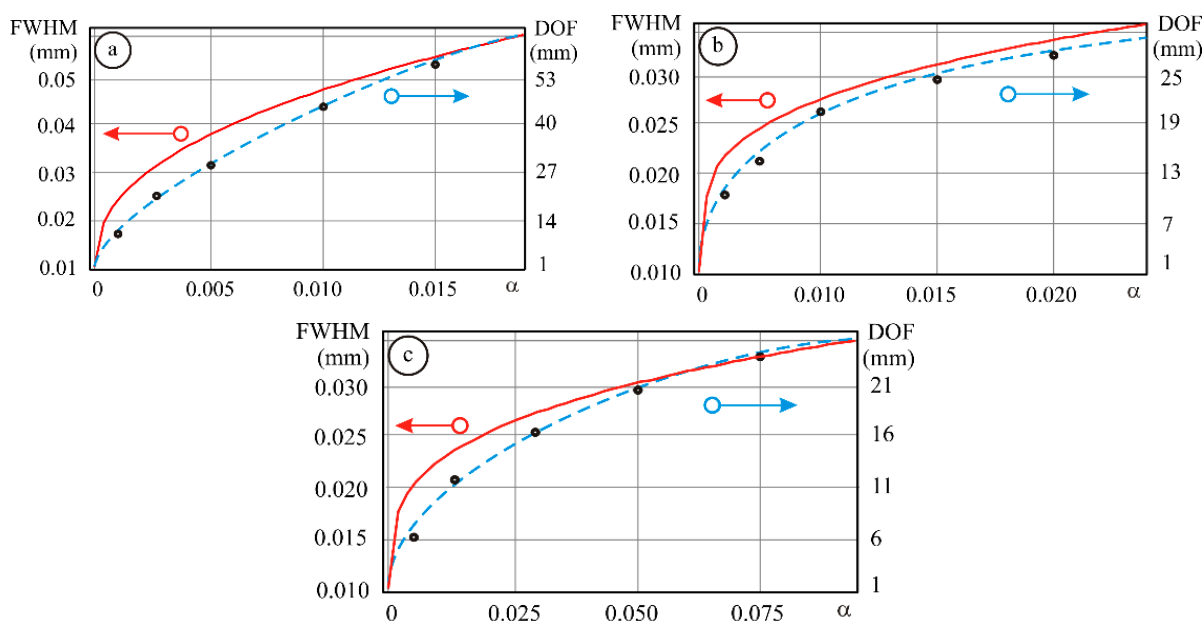


**Figure 5.** Graphs of the dependence of the central light spot size in the focal plane (solid line) and DOF (dashed line) on the coefficient  $\alpha$ : (a)  $n = 3$ , (b)  $n = 4$ , and (c)  $n = 5$ .

When apodization is absent ( $\alpha = 0$ ), a light spot of the minimum diffraction size is observed in the focal plane ( $\text{FWHM} \approx 0.01 \text{ mm}$ ). With increasing  $\alpha$ , the size of the central light spot increases as a nonlinear dependence. The curves for the DOF in Figure 5 start at 1.1 mm ( $\alpha = 0$ ) and are more linear, especially for  $n = 3$  (Figure 5a), where small changes of the parameter  $\alpha$  lead to a significant increase in the DOF. For  $n = 4$  (Figure 5b), the considered characteristics are less sensitive to an increase in  $\alpha$ , and for  $n = 5$  (Figure 5c), the DOF changes very little with a significant change of  $\alpha$ .

In all cases, there are regions of evidential non-linear dependence (at small values of  $\alpha$ ) as well as regions with almost linear dependence. Note that in the region of linear dependence, the rate of increase in the DOF becomes comparable to the rate of increase in the size of the central spot (especially for  $n = 3$  and  $n = 5$ ). Using the constructed dependencies, it is possible to choose the maximum possible  $\alpha$  (providing the highest DOF) with a CoC size limit imposed.

Provided that the size of the central spot is limited to 0.04 mm (i.e., 2 times larger than in the case considered above), it is possible to significantly increase the DOF and take advantage of higher degrees  $n$ . Figures 6 and 7 show the corresponding PSF calculation

results (transverse and longitudinal patterns) for  $\alpha = 0.0015$ . For phase apodization with  $\alpha = 0.0015$  in the focal plane, at  $n = 3$ , FWHM = 0.041 mm and DOF = 51 mm; at  $n = 4$ , FWHM = 0.037 mm and DOF = 41 mm; and at  $n = 5$ , FWHM = 0.034 mm and DOF = 29 mm. Although the dependencies are nonlinear, on average, with an increase in CoC by a factor of 2, the DOF increases by a factor of 8.

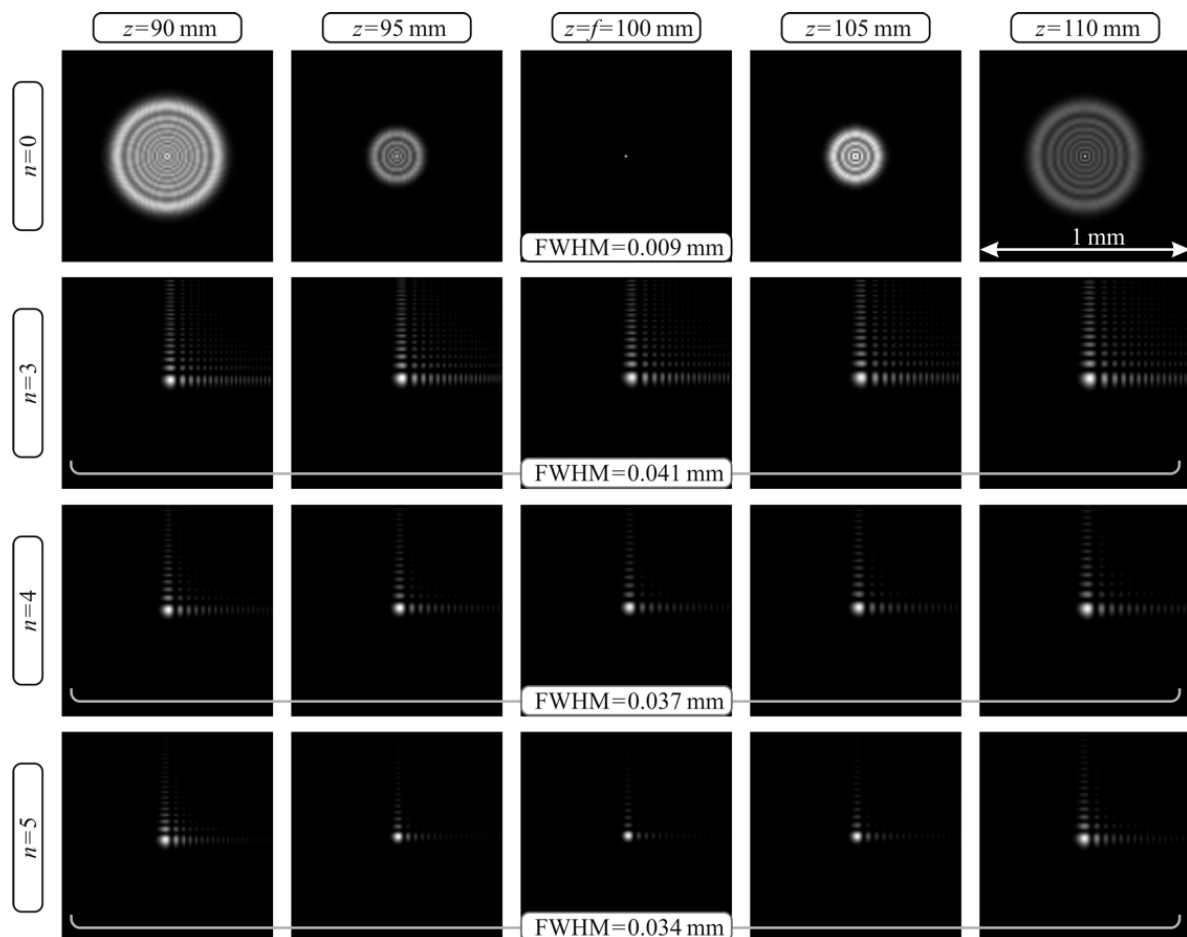


**Figure 6.** PSF with a CoC size limit of 0.04 mm ( $\alpha = 0.0015$ ) at different distances (1 mm  $\times$  1 mm pattern size) for a lens without apodization (first row) and with phase apodization  $n = 3$  (second row),  $n = 4$  (third row), and  $n = 5$  (fourth row), for  $\lambda = 550$  nm.

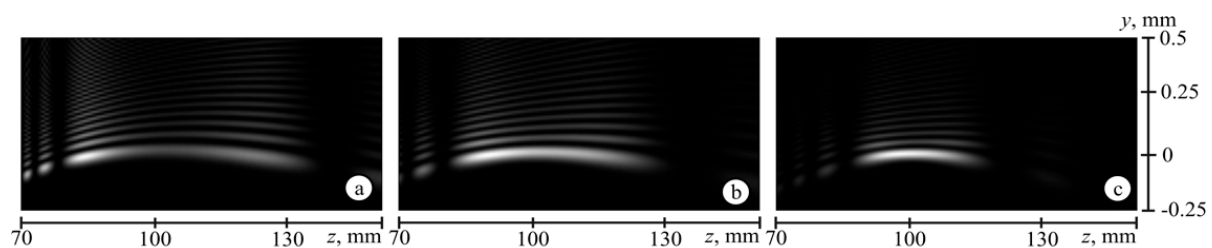


**Figure 7.** PSF longitudinal distribution patterns with a CoC size limit of 0.04 mm,  $\alpha = 0.0015$  for a lens with phase apodization  $n = 3$  (a),  $n = 4$  (b), and  $n = 5$  (c), for  $\lambda = 550$  nm.

The dependencies of the DOF on the degree  $n$  and parameter  $\alpha$  are shown more generally in Figure 8. This figure shows that the distribution of the maximum intensity for  $n = 4$  and  $n = 5$  is more compact (that is, the DOF is less), but much more uniformly than for  $n = 3$ . The uniformity of the distribution in Figure 8 corresponds to the degree of PSF invariance during defocusing. This is an important property of the apodization

function, which makes it possible to use the same distribution when restoring an object during defocusing. Thus, the use of apodization functions with  $n = 4$  and  $n = 5$  provides a more stable PSF during defocusing than with  $n = 3$ . Some reduction in the DOF can be compensated by an additional adjustment of the apodization function by increasing the parameter  $\alpha$ .

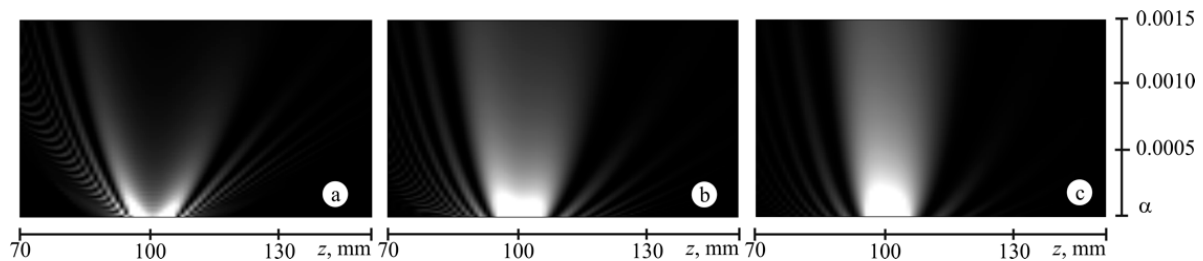


**Figure 8.** The distribution of the maximum intensity depending on the parameter  $\alpha \in [0.0001; 0.0015]$  for various values of  $n$ :  $n = 3$  (a),  $n = 4$  (b), and  $n = 5$  (c), for  $\lambda = 550$  nm.

To compare apodization functions more fully with  $n = 3$  and  $n = 5$ , we also plotted curves of the modulation transfer functions (MTF) in Figure 9. This figure shows that with apodization, spatial resolution significantly deteriorates, especially with an increase in the parameter  $\alpha$ , which is expected and is in full agreement with the above results. Interestingly, on average, for  $n = 5$ , the degradation in spatial resolution is less than that for  $n = 3$ .

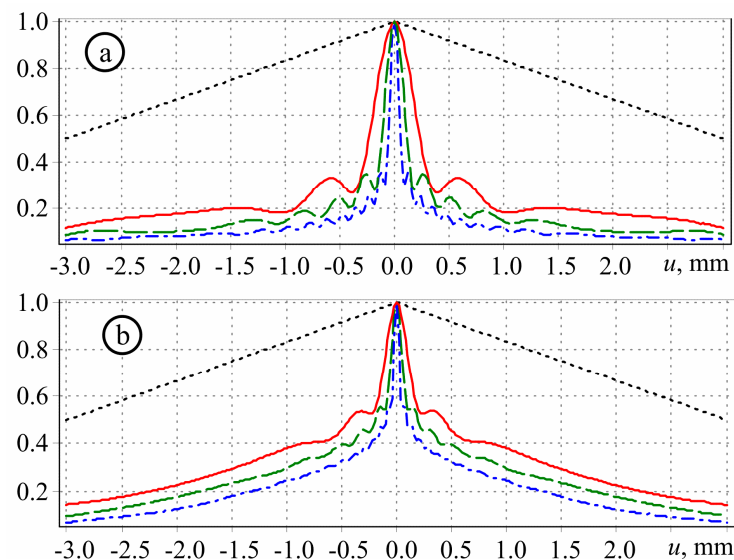


**Figure 9.** The MTF in the focal plane for  $n = 3$  (a) and  $n = 5$  (b) depending on the parameter  $\alpha$ , with  $\alpha = 0$  (without apodization, dotted line),  $\alpha = 0.0005$  (solid line),  $\alpha = 0.001$  (dashed line), and  $\alpha = 0.002$  (dash-dotted line), for  $\lambda = 550$  nm.

### 3. Chromatic Effect

Accounting for the effects of chromatic aberration is also important for imaging systems. Although the compensation of chromatic aberrations is often associated with a deepening of the focus [3,41], for different types of apodization functions, the chromatic effect can have a different influence.

Figure 10 shows the results of calculating the PSF for a lens without apodization and with apodization at three wavelengths of the illuminating beam:  $\lambda = 460$  nm (blue), 550 nm (green), and 640 nm (red). This figure shows that in the absence of apodization, a significant chromatic effect is observed, and this effect is different before and after the focus.

For apodized PSF, chromatism noticeably affects only the side lobes (with a symmetrical effect before and after the focus), whereas the main peak is not prone to chromatism.

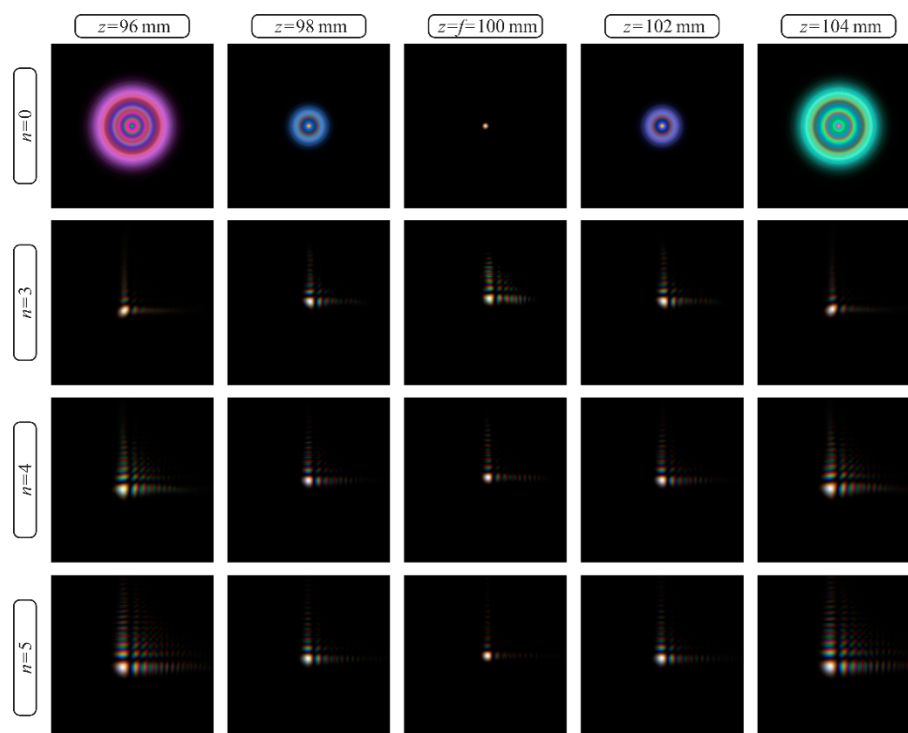


**Figure 10.** PSF at various distances with a CoC size limit of 0.02 mm (0.4 mm × 0.4 mm pattern size) for a lens without apodization (upper row) and with phase apodization  $n = 3$ ,  $\alpha = 0.00045$  (second row);  $n = 4$ ,  $\alpha = 0.00054$  (third row); and  $n = 5$ ,  $\alpha = 0.00081$  (fourth row) at three wavelengths of the illuminating beam:  $\lambda = 460$  nm (blue), 550 nm (green), and 640 nm (red).

For a more visual comparison of the influence of the degree  $n$  of the apodization function, Figure 11 shows patterns of longitudinal distribution of PSF. This figure shows that the depth of focus decreases somewhat with increasing  $n$ , but the PSF distribution becomes more uniform and invariant to defocus, and there is less influence of chromatism.

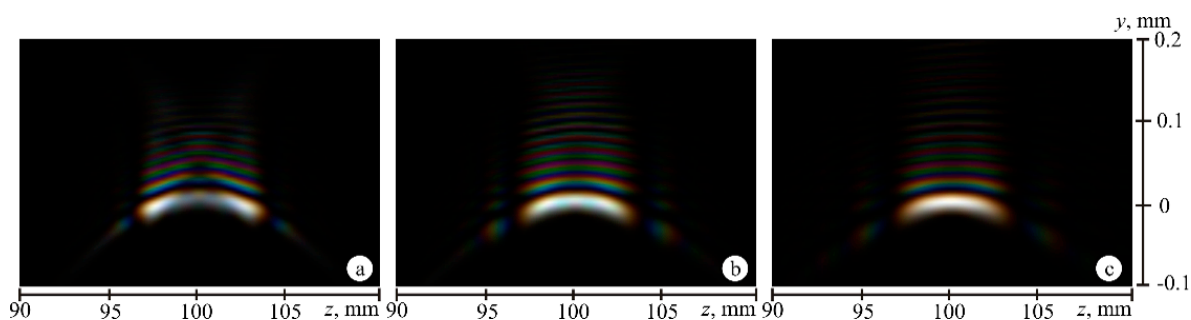


**Figure 11.** PSF longitudinal distribution patterns with a CoC size limit of 0.02 mm ( $z \in [90$  mm; 110 mm],  $y \in [-0.1$  mm; 0.2 mm]) for  $n = 3$ ,  $\alpha = 0.00045$  (a);  $n = 4$ ,  $\alpha = 0.00054$  (b); and  $n = 5$ ,  $\alpha = 0.00081$  (c) at three wavelengths of the illuminating beam:  $\lambda = 460$  nm (blue), 550 nm (green), 640 nm (red).

It is possible to increase the DOF by increasing the coefficient  $\alpha$ , which, as shown in the previous section, also leads to an increase in the size of the central light spot. In this case, a compromise must be sought between the two competing criteria. Figure 12 shows the corresponding results with increased  $\alpha$  (similar to Figure 11). In this case, for apodized PSF, there are practically no differences in the chromatic patterns when shifted

along the optical axis to the left or right. Chromatism mainly affects the side lobes of the apodized PSF. Therefore, the low level of the side lobes at  $n = 4$  and  $n = 5$  becomes even more important.

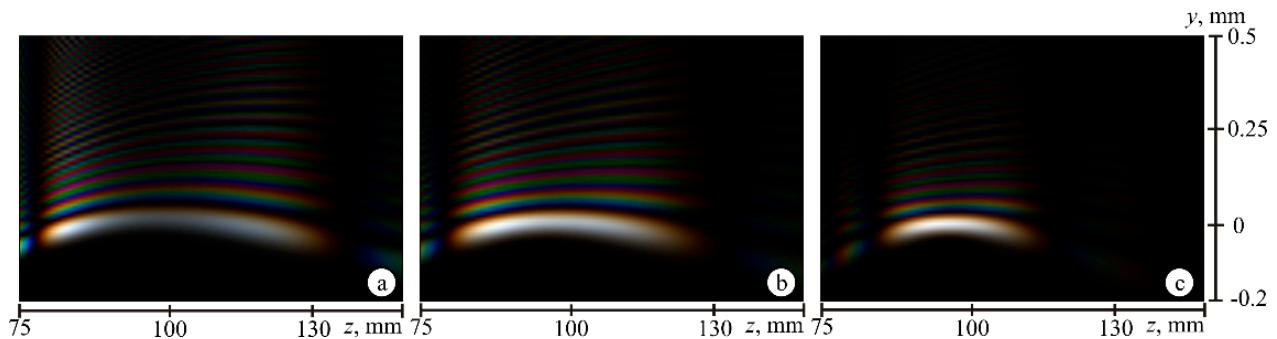


**Figure 12.** PSF longitudinal distribution patterns with a CoC size limit of 0.04 mm,  $\alpha = 0.0015$  ( $z \in [75 \text{ mm}; 150 \text{ mm}]$ ,  $y \in [-0.2 \text{ mm}; 0.5 \text{ mm}]$ ) for a phase apodized lens  $n = 3$  (a),  $n = 4$  (b), and  $n = 5$  (c) at three wavelengths of the illuminating beam:  $\lambda = 460 \text{ nm}$  (blue),  $550 \text{ nm}$  (green),  $640 \text{ nm}$  (red).

According to the calculation results, the higher the degree  $n$ , the better the invariant characteristics of the PSF; i.e., the PSF is less dependent on defocusing, but the DOF is reduced at the same time. This reduction can be compensated by increasing the parameter  $\alpha$ , which in turn leads to an increase in the size of the light spot. In this case, a nonlinear relationship between the increase in the DOF and the spot size  $s$  should be noted (due to a small increase in  $s$ , the DOF can be significantly increased). Thus, depending on the restrictions on the CoC, it is possible to provide a compromise solution to the problem by selecting the parameters of the apodizing function (5).

#### 4. Image Decoding

Figure 13 shows a color test image, which was divided into three components corresponding to RGB channels. Then, each color component was convolved with the corresponding PSF both in the focal plane ( $z = f = 100 \text{ mm}$ ) and outside the focal plane (the  $z = 120 \text{ mm}$  plane was chosen). Simulation results of image formation for the lens without apodization and with asymmetric phase apodization are shown in Figure 14.



**Figure 13.** Test color image.

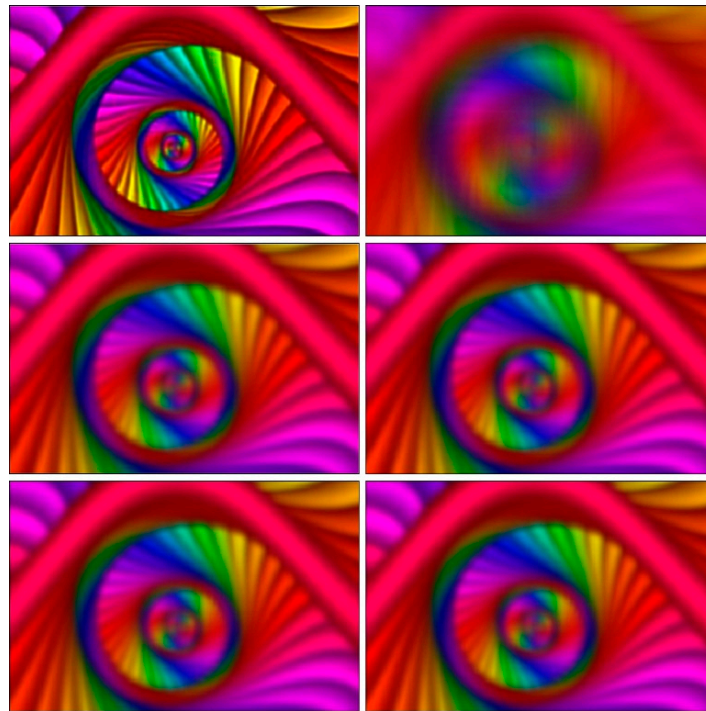


**Figure 14.** Simulation of image formation for a lens without apodization (**upper row**) and with phase apodization  $n = 3$  (**middle row**) and  $n = 4$  (**lower row**) in the focal plane  $z = f = 100$  mm (**left column**) and outside the focal plane  $z = 120$  mm (**right column**).

The image deconvolution was performed by the Richardson–Lucy (R–L) algorithm. The R–L algorithm [56,57] is an iterative technique that attempts to maximize the likelihood of the restored image by using the expectation-maximization method. The algorithm uses information about the process by which the image is degraded. The degradation is described by the PSF of the system.

The image degradation in this work is modelled as  $g(x) = h(x) * f(x)$ , where  $f$  is the original undistorted image,  $g$  is the distorted image,  $h$  is the PSF of the system, and  $*$  is the convolution operator.

An iteration of the R–L algorithm can be written in terms of convolutions:

$$f_{k+1}(x) = f_k(x) \left( h(-x) * \frac{g(x)}{f_k(x) * h(x)} \right), \quad (7)$$

The PSF  $h(x)$  is known, so the estimation of the original image  $f(x)$  is found by iterating (7) until convergence.

Figure 15 shows the results of deconvolution using the R–L method. The reconstructed image for the lens without apodization outside the focal plane ( $z = 120$  mm) is demonstrated in the upper row. On the left, PSF in the same plane ( $z = 120$  mm) is used for restoration. The accuracy of deconvolution, measured as the peak signal-to-noise ratio (PSNR), is 23.1 dB. The color difference CIEDE2000 between the images is 3.1.

On the right in the upper row, PSF in the focal plane is used for reconstruction (PSNR = 18 dB, CIEDE2000 = 4.5). The second and third rows of Figure 15 show the results of deconvolution for a lens with phase apodization  $n = 3$  (middle row) and  $n = 4$  (lower row) outside the focal plane ( $z = 120$  mm). On the left, for PSF with  $z = 120$  mm, the PSNR is 25.2 dB ( $n = 3$ ) and 25.0 dB ( $n = 4$ ), and the CIEDE2000 is 2.6 ( $n = 3$ ) and 2.7 ( $n = 4$ ). On the right, for the PSF in the focal plane, the PSNR is 25.7 dB ( $n = 3$ ) and 25.4 dB ( $n = 4$ ), and the CIEDE2000 is 2.3 ( $n = 3$ ) and 2.4 ( $n = 4$ ).

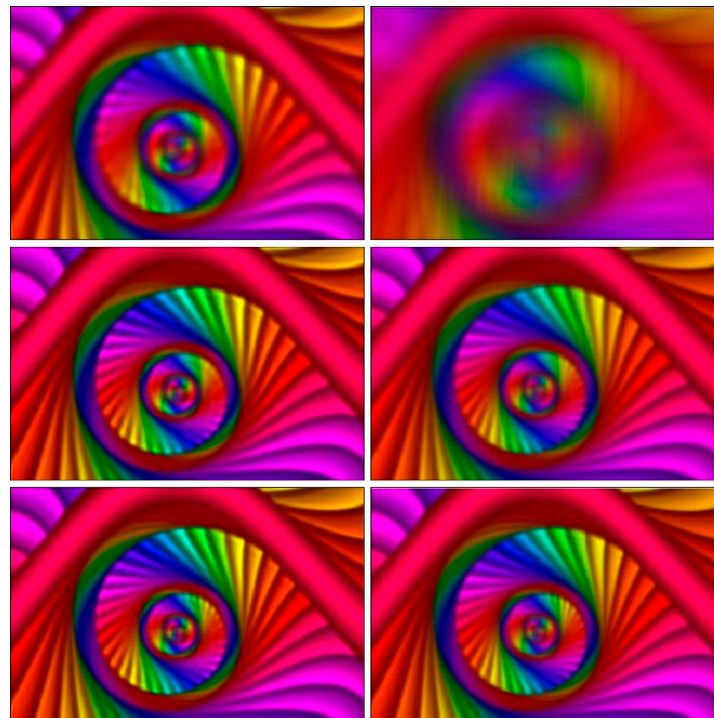


**Figure 15.** Modeling image deconvolution outside the focal plane ( $z = 120$  mm) for a lens without apodization (upper row) and with phase apodization  $n = 3$  (middle row) and  $n = 4$  (lower row) using PSF at  $z = 120$  mm plane (left column) and PSF in the focal plane  $z = f = 100$  mm (right column).

Thus, the comparative results of apodization for  $n = 3$  and  $n = 4$  show the possibility of obtaining very similar results for apodizing functions with different degrees of power due to variations of the scale parameter. However, a higher degree provided slightly better results under moderate defocusing conditions (20% of the focus value), which is in agreement with the analysis performed in the previous sections.

## 5. Conclusions

In this work, we performed a detailed comparative study of the properties of high-order parametric power phase apodization (cubic, fourth-, and fifth-degree) for the compensation of defocusing and chromatic aberration in the imaging system. The research results showed that an increase in the degree of apodization function provided better independence of the PSF from defocusing, but it also reduced the DOF. This reduction could be compensated by increasing the parameter  $\alpha$ ; however, this led to an increase in the size of the light spot. A nonlinear relationship between the increase in the DOF and spot size was shown (due to a small increase in the size of the light spot, the DOF could be significantly increased). Thus, the search for the best solution is based on a compromise of restrictions on the CoC and DOF. For the considered apodization functions, modeling of the formation of a color image under defocusing conditions with subsequent deconvolution of the resulting image was performed. Comparative results showed the possibility of obtaining very close results for apodizing functions with different degrees of power due to variations of the scale parameter. However, a higher degree provided slightly better results in moderate defocusing conditions.

**Author Contributions:** Conceptualization, S.N.K., P.G.S. and S.B.P.; methodology, S.N.K., P.G.S. and S.B.P.; software, S.G.V., A.P.D. and P.G.S.; validation, S.N.K., S.G.V. and A.P.D.; formal analysis, S.N.K., P.G.S. and M.A.B.; investigation, S.N.K., S.G.V., A.P.D. and P.G.S.; resources, S.N.K., S.B.P. and M.A.B.; data curation, S.G.V., A.P.D. and P.G.S.; writing—original draft preparation, S.N.K., P.G.S. and M.A.B.; writing—review and editing, S.N.K., P.G.S., S.B.P. and M.A.B.; visualization, S.N.K., S.G.V., A.P.D. and P.G.S.; supervision, S.N.K. and S.B.P.; project administration, P.G.S. and S.B.P.;

funding acquisition, S.B.P. and M.A.B. All authors have read and agreed to the published version of the manuscript.

**Funding:** The reported study was funded by RFBR, project number 19-29-09054, for machine learning for digital decoding operation; by the Ministry of Science and Higher Education of the Russian Federation under the state task of the Federal Research Center “Crystallography and Photonics” RAS (agreement No. 007-GZ/Ch3363/26) for aberrated wavefront modeling and PSF calculations; and under the Scientific State assignment of the Samara National Research University (No. 0777-2020-0017) for comparative analysis.

**Acknowledgments:** We acknowledge the equal contribution of all the authors.

**Conflicts of Interest:** The authors declare no conflict of interest.

## References

1. Dowski, E.R.; Cathey, W.T. Extended depth of field through wave-front coding. *Appl. Opt.* **1995**, *34*, 1859–1866. [[CrossRef](#)]
2. Van der Gracht, J.; Dowski, E.R.; Taylor, M.G.; Deaver, D.M. Broadband behavior of an optical-digital focus-invariant system. *Opt. Lett.* **1996**, *21*, 919–921. [[CrossRef](#)]
3. Wach, H.; Dowski, E.R.; Cathey, W.T. Control of chromatic focal shift through wavefront coding. *Appl. Opt.* **1998**, *37*, 5359–5367. [[CrossRef](#)]
4. Pan, C.; Chen, J.; Zhang, R.; Zhuang, S. The extension ratio of depth of field by wavefront coding method. *Opt. Express* **2008**, *16*, 13364–13371. [[CrossRef](#)]
5. Tucker, S.C.; Cathey, W.T.; Dowski, E.R. Extended depth of field and aberration control for inexpensive digital microscope systems. *Opt. Express* **1999**, *4*, 467–474. [[CrossRef](#)]
6. Zhang, W.Z.; Ye, Z.; Chen, Y.P.; Zhao, T.Y.; Yu, F.H. Ray aberrations analysis for phase plates illuminated by off-axis collimated beams. *Opt. Express* **2007**, *15*, 3031–3046. [[CrossRef](#)] [[PubMed](#)]
7. Yan, F.; Zheng, L.G.; Zhang, X.J. Image restoration of an off-axis three-mirror anastigmatic optical system with wavefront coding technology. *Opt. Eng.* **2008**, *47*, 8. [[CrossRef](#)]
8. Wang, H.; Gan, F. High focal depth with a pure-phase apodizer. *Appl. Opt.* **2001**, *40*, 5658–5662. [[CrossRef](#)]
9. Sherif, S.S.; Cathey, W.T.; Dowski, E.R. Phase plate to extend the depth of field of incoherent hybrid imaging systems. *Appl. Opt.* **2004**, *43*, 2709–2721. [[CrossRef](#)]
10. Castro, A.; Ojeda-Castaneda, J. Asymmetric phase masks for extended depth of field. *Appl. Opt.* **2004**, *43*, 3474–3479. [[CrossRef](#)]
11. Xu, Y.; Singh, J.; Sheppard, C.J.R.; Chen, N. Ultra long high resolution beam by multi-zone rotationally symmetrical complex pupil filter. *Opt. Express* **2007**, *15*, 6409–6413. [[CrossRef](#)] [[PubMed](#)]
12. Bagheri, S.; Javidi, B. Extension of depth of field using amplitude and phase modulation of the pupil function. *Opt. Lett.* **2008**, *33*, 757–759. [[CrossRef](#)]
13. Khonina, S.N. Phase apodization of imaging system to increase the focal depth in coherent and incoherent cases. *Comput. Opt.* **2012**, *36*, 357–364.
14. Lyu, Q.; Zhai, Z.; Sharp, M.; French, P. The extended depth of field microscope imaging system with the phase pupil mask. *Proc. SPIE* **2015**, 9795. [[CrossRef](#)]
15. Khonina, S.N.; Ustinov, A.V. Generalized apodization of an incoherent imaging system aimed for extending the depth of focus. *Pattern Recognit. Image Anal.* **2015**, *25*, 626–631. [[CrossRef](#)]
16. Jacquinot, P.; Roizen-Dossier, B. Apodization. *Prog. Opt.* **1964**, *3*, 29–186.
17. Kant, R. Superresolution and increased depth of focus: an inverse problem of vector diffraction. *J. Mod. Opt.* **2000**, *47*, 905–916. [[CrossRef](#)]
18. Khonina, S.N.; Ustinov, A.V.; Pelevina, E.A. Analysis of wave aberration influence on reducing the focal spot size in a high-aperture focusing system. *J. Opt.* **2011**, *13*, 095702. [[CrossRef](#)]
19. Sun, C.-C.; Liu, C.-K. Ultrasmall focusing spot with a long depth of focus based on polarization and phase modulation. *Opt. Lett.* **2003**, *28*, 99–101. [[CrossRef](#)]
20. Liu, Z.; Flores, A.; Wang, M.R.; Yang, J.J. Diffractive infrared lens with extended depth of focus. *Opt. Eng.* **2007**, *46*, 018002. [[CrossRef](#)]
21. Lerman, G.M.; Levy, U. Effect of radial polarization and apodization on spot size under tight focusing conditions. *Opt. Express* **2008**, *16*, 4567–4581. [[CrossRef](#)]
22. Khonina, S.N. Simple phase optical elements for narrowing of a focal spot in high-numerical-aperture conditions. *Opt. Engineer.* **2013**, *52*, 091711. [[CrossRef](#)]
23. Liu, X.; Cai, X.; Chang, S.; Grover, C.P. Cemented doublet lens with an extended focal depth. *Opt. Express* **2005**, *13*, 552–557. [[CrossRef](#)]
24. Yun, M.; Lee, E.-H. Focal shift and extended focal depth with tunable pupil filter. *J. Mod. Opt.* **2008**, *55*, 2857–2863. [[CrossRef](#)]
25. Khonina, S.N.; Ustinov, A.V.; Porfirev, A.P. Dynamic focal shift and extending depth of focus based on the masking of the illuminating beam and using an adjustable axicon. *J. Opt. Soc. Am. A* **2019**, *36*, 1039–1047. [[CrossRef](#)] [[PubMed](#)]

26. Siu, G.G.; Cheng, L.; Chiu, D.S. Improved side-lobe suppression in asymmetric apodization. *J. Phys. D Appl. Phys.* **1994**, *27*, 459–463. [CrossRef]
27. Khonina, S.N.; Volotovskiy, S.G. Minimization of light or dark focal spot size with controllable growth of side lobes in focusing systems with the high numerical aperture. *Comput. Opt.* **2011**, *35*, 438–451.
28. Reddick, R.C.; Warmark, R.J.; Ferrel, T.L. New form of scanning optical microscopy. *Phys. Rev. B* **1989**, *39*, 767–770. [CrossRef] [PubMed]
29. Kowalczyk, M.; Zapata-Rodriguez, C.J.; Martinez-Corral, M. Asymmetric apodization in confocal scanning systems. *Appl. Opt.* **1998**, *37*, 8206–8214. [CrossRef]
30. Hecht, B.; Sick, B.; Wild, U.P.; Deckert, V.; Zenobi, R.; Martin, O.J.F.; Pohl, D.W. Scanning near-field optical microscopy with aperture probes: fundamentals and applications. *J. Chem. Phys.* **2000**, *112*, 7761–7774. [CrossRef]
31. Boruah, B.R.; Neil, M.A.A. Laser scanning confocal microscope with programmable amplitude, phase, and polarization of the illumination beam. *Rev. Sci. Instrum.* **2009**, *80*, 013705. [CrossRef] [PubMed]
32. Fürhapter, S.; Jesacher, A.; Bernet, S.; Ritsch-Marte, M. Spiral phase contrast imaging in microscopy. *Opt. Express* **2005**, *13*, 689–694. [CrossRef] [PubMed]
33. Situ, G.; Warber, M.; Pedrini, G.; Osten, W. Phase contrast enhancement in microscopy using spiral phase filtering. *Opt. Commun.* **2010**, *283*, 1273. [CrossRef]
34. Maurer, C.; Jesacher, A.; Bernet, S.; Ritsch-Marte, M. What spatial light modulators can do for optical microscopy. *Laser Photonics Rev.* **2011**, *5*, 81–101. [CrossRef]
35. Asakura, T.; Ueno, T. Apodization for increasing two-point resolution by the sparrow criterion under the partially coherent illumination. *Nouvelle Revue d'Optique* **1974**, *5*, 349–359. [CrossRef]
36. Reddy, A.N.K.; Sagar, D.K.; Khonina, S.N. Complex pupil masks for aberrated imaging of closely spaced objects. *Opt. Spectrosc.* **2017**, *123*, 940–949. [CrossRef]
37. Reddy, A.N.K.; Khonina, S.N. Apodization for improving the two-point resolution of coherent optical systems with defect of focus. *Appl. Phys. B* **2018**, *124*, 229. [CrossRef]
38. Raveh, I.; Mendlovic, D.; Zalevsky, Z.; Lohmann, A.W. Digital method for defocus correction: experimental results. *Opt. Eng.* **1999**, *38*, 1620–1626. [CrossRef]
39. Cathey, W.T.; Dowski, E.R. New paradigm for imaging systems. *Appl. Opt.* **2002**, *41*, 6080–6092. [CrossRef]
40. Asif, M.S.; Ayremlou, A.; Sankaranarayanan, A.; Veeraraghavan, A.; Baraniuk, R.G. FlatCam: Thin, lensless cameras using coded aperture and computation. *IEEE Trans. Comput. Imaging* **2017**, *3*, 384–397. [CrossRef]
41. Sitzmann, V.; Diamond, S.; Peng, Y.; Dun, X.; Boyd, S.; Heidrich, W.; Heide, F.; Wetzstein, G. End-to-end optimization of optics and image processing for achromatic extended depth of field and super-resolution imaging. *ACM Trans. Graph.* **2018**, *37*, 114. [CrossRef]
42. Hershko, E.; Weiss, L.E.; Michaeli, T.; Shechtman, Y. Multicolor localization microscopy and point-spread-function engineering by deep learning. *Opt. Express* **2019**, *27*, 6158–6183. [CrossRef] [PubMed]
43. Xu, L.; Ren, J.S.J.; Liu, C.; Jia, J. Deep convolutional neural network for image deconvolution. In *Advances in Neural Information Processing Systems*; MIT Press: Cambridge, MA, USA, 2014; pp. 1790–1798.
44. Eilertsen, G.; Kronander, J.; Denes, G.; Mantiuk, R.; Unger, J. HDR image reconstruction from a single exposure using deep CNNs. *ACM Trans. Graph.* **2017**, *36*, 178. [CrossRef]
45. Zhao, H.; Gallo, O.; Frosio, I.; Kautz, J. Loss functions for image restoration with neural networks. *IEEE Trans. Comput. Imaging* **2017**, *3*, 47–57. [CrossRef]
46. Elmalem, S.; Giryas, R.; Marom, E. Learned phase coded aperture for the benefit of depth of field extension. *Opt. Express* **2018**, *26*, 15316–15331. [CrossRef]
47. Marks, D.L.; Stack, R.A.; Brady, D.J. Three-dimensional tomography using a cubic-phase plate extended depth-of-field system. *Opt. Lett.* **1999**, *24*, 253–255. [CrossRef]
48. Narayanswamy, R.; Johnson, G.E.; Silveira, P.E.X.; Wach, H.B. Extending the imaging volume for biometric iris recognition. *Appl. Opt.* **2005**, *44*, 701–712. [CrossRef]
49. Silveira, P.E.X.; Narayanswamy, R. Signal-to-noise analysis of task-based imaging systems with defocus. *Appl. Opt.* **2006**, *45*, 2924–2934. [CrossRef]
50. Simonov, A.N.; Vdovin, G.; Rombach, M.C. Cubic optical elements for an accommodative intraocular lens. *Opt. Express* **2006**, *14*, 7757–7775. [CrossRef]
51. Khonina, S.N.; Ustinov, A.V.; Skidanov, R.V.; Porfirev, A.P. Local foci of a parabolic binary diffraction lens. *Appl. Opt.* **2015**, *54*, 5680–5685. [CrossRef]
52. Born, M.; Wolf, E. *Principle of Optics*, 7th ed.; Cambridge University: Cambridge, UK, 1999.
53. Flores, A.; Wang, M.R.; Yang, J.J. Achromatic hybrid refractive–diffractive lens with extended depth of focus. *Appl. Opt.* **2004**, *43*, 5618–5630. [CrossRef]
54. Ustinov, A.V.; Khonina, S.N. Generalized lens: Calculation of distribution on the optical axis. *Comput. Opt.* **2013**, *37*, 307–315. [CrossRef]
55. Available online: [https://en.wikipedia.org/wiki/Circle\\_of\\_confusion](https://en.wikipedia.org/wiki/Circle_of_confusion); <http://www.rags-int-inc.com/PhotoTechStuff/DoF/> (accessed on 1 May 2021).

- 
56. Richardson, W.H. Bayesian-based iterative method of image restoration. *J. Opt. Soc. Am.* **1972**, *2*, 55–59. [[CrossRef](#)]
  57. Lucy, L.B. An iterative technique for the rectification of observed images. *Astron. J.* **1974**, *79*, 745–754. [[CrossRef](#)]